SLAC-PUB-3260
November 1983
(E)

RECENT RESULTS FROM DELCO*

W. B. Atwood, P. H. Baillon, B. C. Barish, G. R. Bonneaud,
H. DeStaebler, G. J. Donaldson, R. Dubois, M. M. Duro, E. Elsen, S. G. Gao,
Y. Z. Huang, G. M. Irwin, R. P Johnson, H. Kichimi, J. Kirkby, D. E. Klem,
D. E. Koop, J. Ludwig, G. B. Mills, A. Ogawa, T. Pal, D. Perret-Gallix,
R. Pitthan, D. L. Pollard, C. Y. Prescott, L. Z. Rivkin, L. S. Rochester,
W. Ruckstuhl, M. Sakuda, S. S. Sherman, E. J. Siskind, R. Stroynowski,
S. Q. Wang, S. G. Wojcicki, H. Yamamoto, W. G. Yen and C. C. Young

Presented by Charles C. Young

California Institute of Technology, Pasadena, California 91125
Stanford Linear Accelerator Center and Physics Department
Stanford University, Stanford, California 94305

Presented at the 11th SLAC Summer Institute on Particle Physics
Stanford, California, July 18–29, 1983

* Work supported by the Department of Energy, contract numbers DE-AC03-76SF00515 (SLAC) and DE-AC03-81-ER40050 (CIT), and The National Science Foundation.

1. Introduction

DELCO is a magnetic spectrometer with Čerenkov, Time-of-Flight (TOF) and shower counters for particle identification. It is located in IR8 of the PEP storage ring. Data have been obtained at a center of mass energy, $\sqrt{s}$, of 29 GeV. We report on:

1) the fraction of P, K, π in hadronic events,

2) the observation of direct electron signals, and

3) the measurement of D^* fragmentation function and its total cross-section.

2. Detector

DELCO is a magnetic detector with drift chambers for tracking, and Čerenkov, Time-of-Flight, and shower counters for particle identification. See Figures 1 and 2. The magnetic field is generated by two coils. A total bending strength of .18 T-m imparts 50 MeV/c transverse momentum to charged particles. There are 16 layers in the two drift chambers around the beam pipe, and each layer has a position resolution of 160 μm. There are six more layers of drift chambers at $r \simeq 1.5$ m. This results in a momentum resolution $\sigma_p/p = \sqrt{.06^2 + (.02p)^2}$, where p is the momentum in GeV/c. The inverse momentum distribution of Bhabha tracks is shown in Figure 3.

The 36-cell Čerenkov counter is situated between the two sets of drift chambers. It is operated at atmospheric pressure, and was filled with isobutane (nitrogen) for 80% (20%) of the data. Čerenkov light is focused by ellipsoidal mirrors onto RCA 8854 Quantacon photomultiplier tubes. The use of ellipsoidal mirrors results in isochronous signals for particles coming from the origin. Timing resolution of 300 psec (450 psec) was achieved for isobutane (nitrogen) radiator. Other stray particles can be discriminated against on the basis of timing. The single-photoelectron capability of the photomultiplier and the relatively high light yield of 26(5) photoelectrons made the Čerenkov counter efficient. Figure 4 shows the measured light yield of 10.6 K Bhabha tracks. Two tracks registered no pulse height, corresponding to an inefficiency of .02%. For momentum below 200 MeV/c, there is an inefficiency due to track curvature.

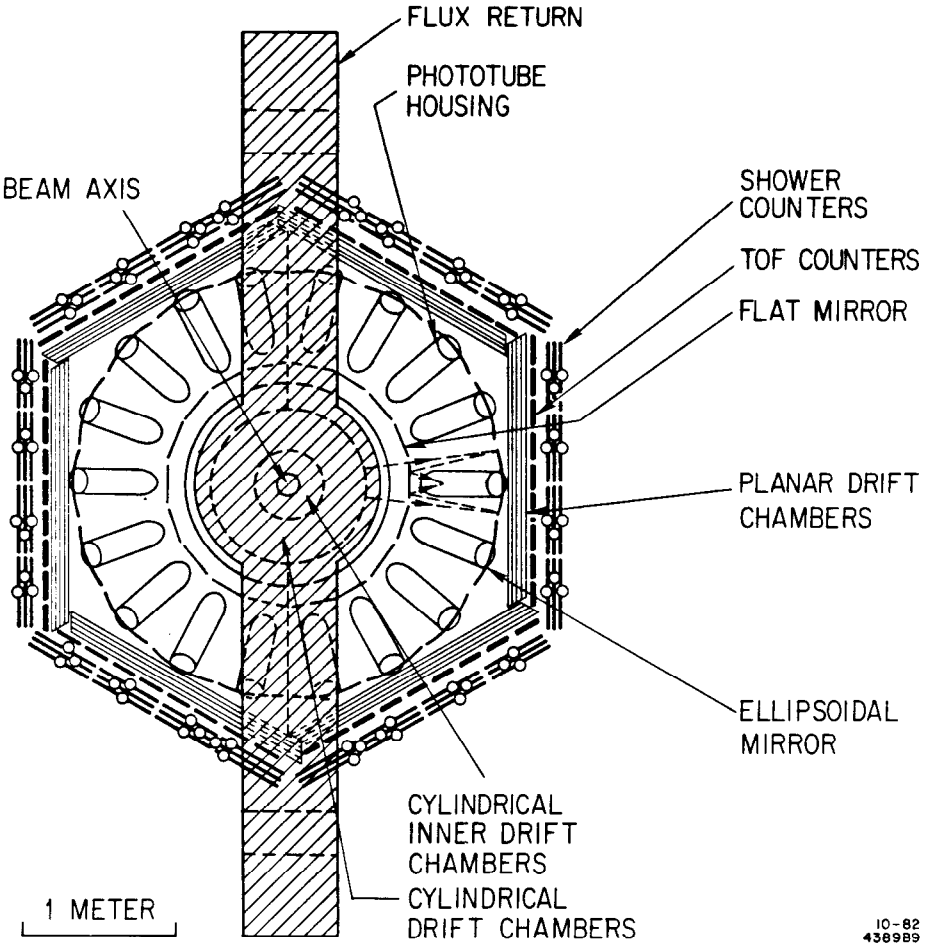

Figure 1 Plan view of DELCO detector.

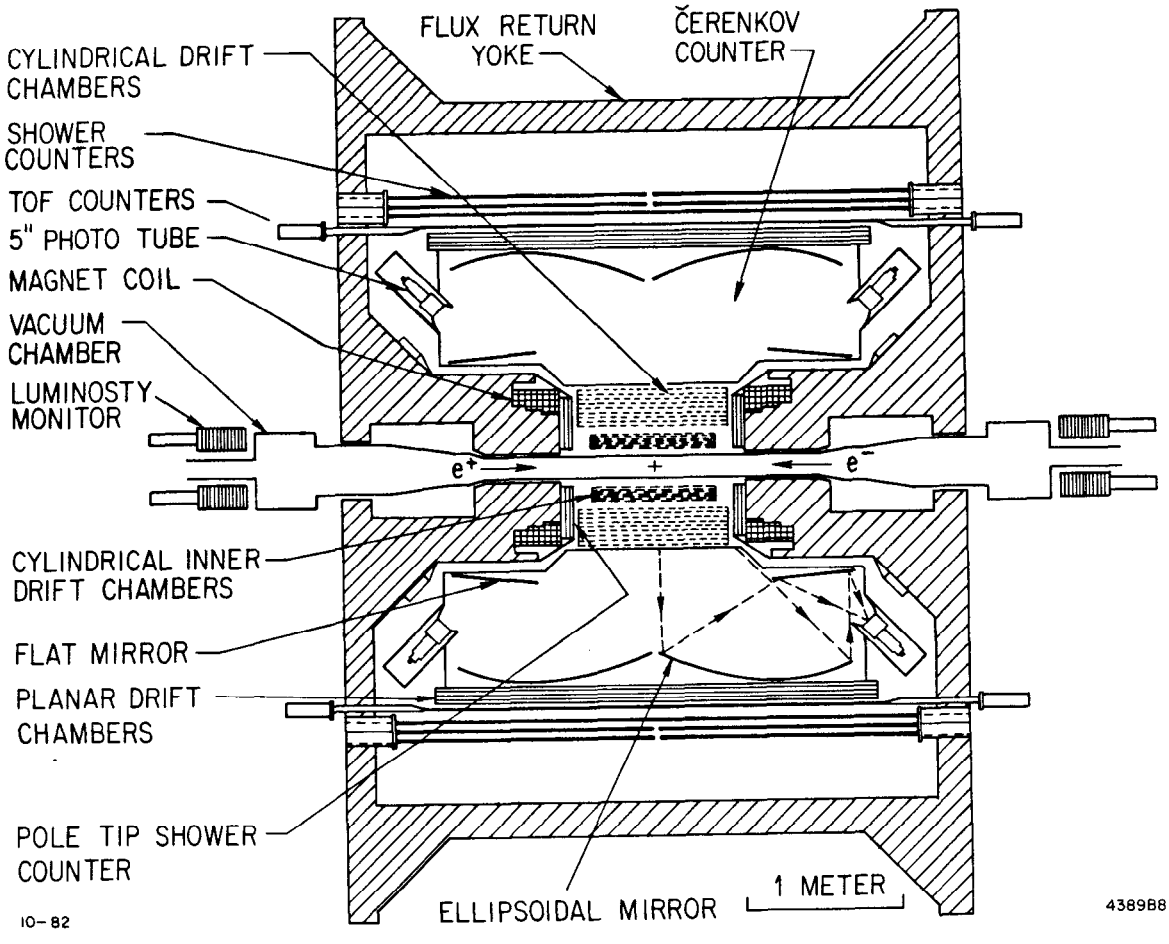

Figure 2 End view of DELCO detector.

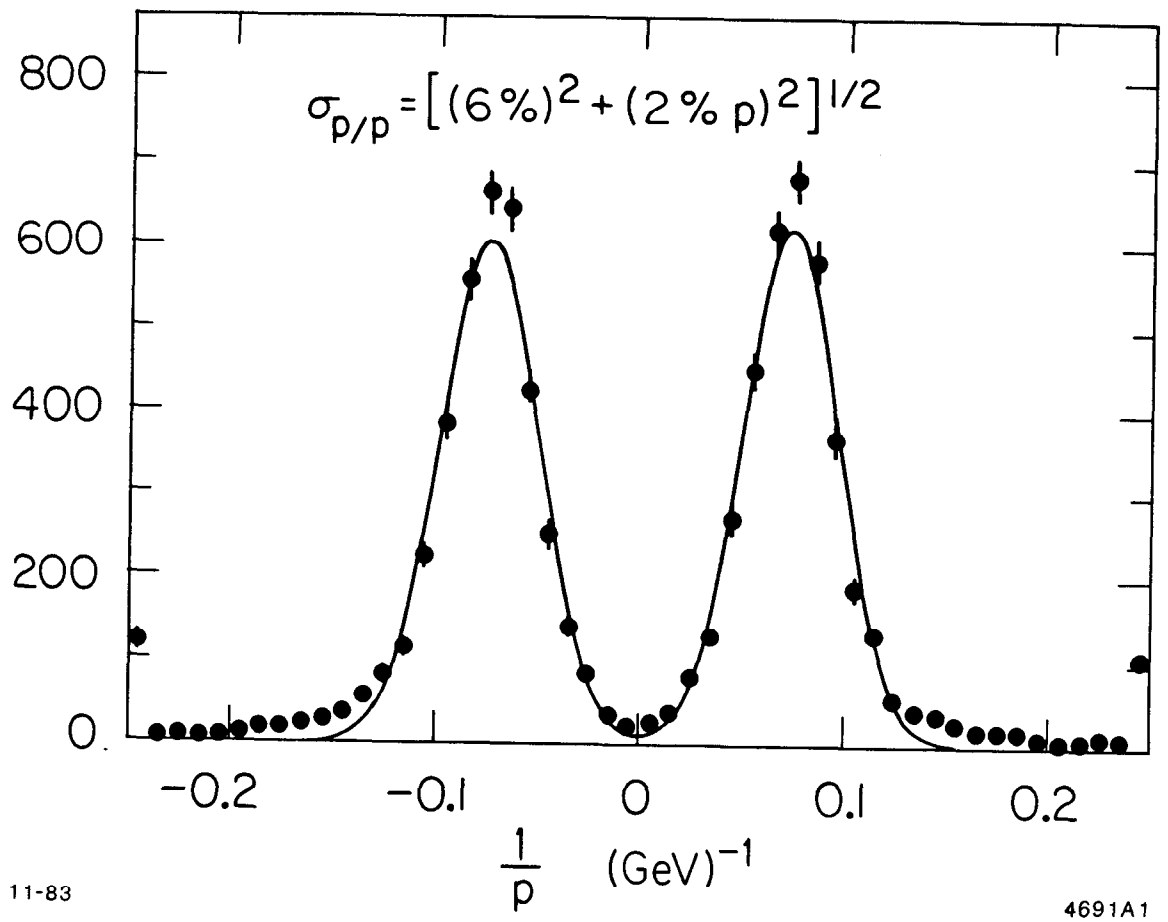

Figure 3 1/p of Bhabha tracks.

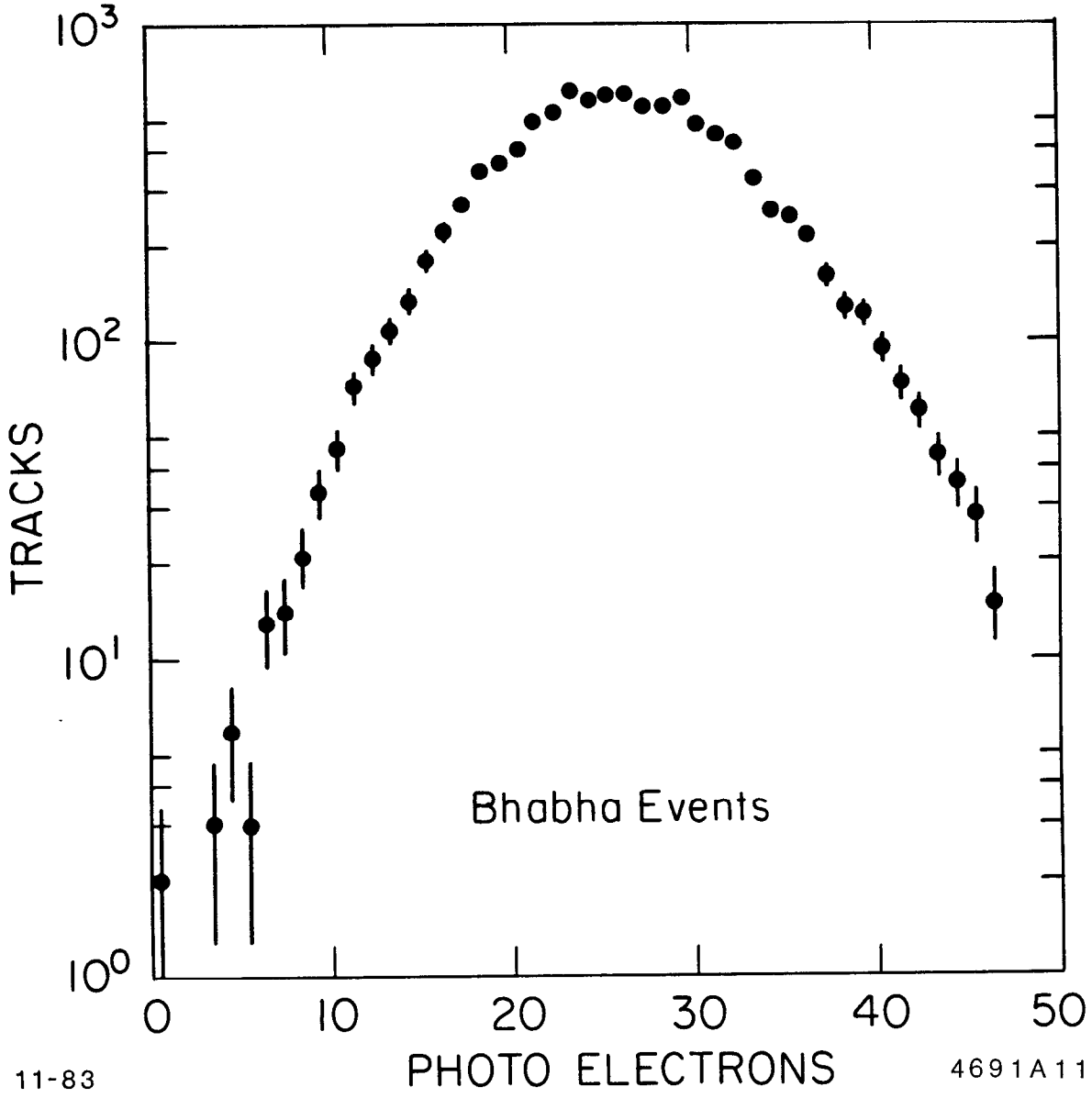

Figure 4 Čerenkov pulse height distribution in Bhabha events. Response has been normalized to 100 cm path length.

There are 52 TOF counters outside the outer drift chambers. Each counter is viewed at both ends, and a timing resolution of 300 psec is achieved in low multiplicity events. The resolution in hadronic events is 350 psec.

There are 48 shower counters outside the TOF counters. They are made of lead-scintillator sandwiches, and are read out at three different depths: two, four and six radiation lengths (X_0).

There are 36 shower counters mounted on the two pole-tips, covering the angular range $.79 < |\cos\vartheta| < .98$. These are 5-$X_0$ lead-scintillator sandwiches, and the light is read out using wave-shifter bars.

The luminosity counters cover the region 25 mrad $< \vartheta <$ 68 mrad. These 16-X_0 counters are divided into six azimuthal pairs. Their construction and read-out are similar to the pole-tip shower counters.

The open geometry of the detector ensures that there is little material (.05 X_0) before the Čerenkov counter. This minimizes photon conversion and therefore the background in the Čerenkov counter. Table 1 summarizes the material before the Čerenkov counter.

Table 1

Summary of Material Before Čerenkov Counter				
	Material	Thickness cm	Thickness X_0	Total Thickness X_0
Beam Pipe	Al	0.2	2.2 %	2.2 %
Drift Chamber			1.8 %	4.0 %
Čerenkov Entrance Window	Al	0.07	0.8 %	4.8 %
Čerenkov Gas	Isobutane	85	0.5 %	5.3 %

A summary of the detector's acceptance and performance is given in Table 2.

Table 2

Summary of the Acceptance and Performance of the DELCO Detector	
Magnet	Open-geometry (aperture $\lvert\cos\vartheta\rvert < 0.78$) Pole-tip diameter 101 cm, separation 125 cm $B_0 = 3.3$ kG, $\int Bdl = 1.8$ kG m
Tracking	Central (cylindrical) drift chambers: 94 cm maximum wire length, 12–49 cm radius Low mass (2.3 % X_0) Depth (z) measurement by narrow angle stereo 16 points on tracks with $\lvert\cos\vartheta\rvert < 0.69$ Outer (planar) drift chambers: 285 cm wire length, 160 cm (radius) Depth measurement by wide angle stereo 6 points on tracks with $\lvert\cos\vartheta\rvert < 0.65$ Multiple hit digital electronics (4 nsec bin width) $\sigma_p/p = \sqrt{(2\%\ p)^2 + (6\%)^2}$
Čerenkov Counter	1 atm isobutane threshold counter ($\gamma_t = 19.1$) 36 cells each with (pTP–coated) 5" RCA 8854 Quantacon Radiator length 55–110 cm $\langle pe\rangle = 26, \langle N_0\rangle = 80$ cm^{-1} $\sigma_t = 300$ psec Acceptance $\lvert\cos\vartheta\rvert < 0.62$
Shower Counters	Barrel ($\lvert\cos\vartheta\rvert < 0.62$): 48 Pb–scintillator counters, $6X_0$ Pole-tip ($0.79 < \lvert\cos\vartheta\rvert < 0.98$): 36 Pb–scintillator BBQ counters, $5X_0$
Time-of-Flight	52 counters 324 cm length, 180 cm (radius) $\sigma_t = 350$ psec Acceptance $\lvert\cos\vartheta\rvert < 0.67$
Luminosity Monitor	12 Pb–scintillator BBQ counters, 16 X_0 Acceptance 25–68 mrad relative to beam axis

3. Data

Data were collected in 1982 and 1983 at $\sqrt{s} = 29$ GeV. A total luminosity of 116 pb^{-1}, corresponding to $\simeq 53$K hadrons, was recorded.

Approximately 80% of the data was taken with isobutane as the Čerenkov radiator; while for the remaining 20%, the Čerenkov counter was filled with nitrogen. Pion threshold is 2.6 GeV/c (5.6 GeV/c) in isobutane (nitrogen). Thus in the isobutane data, electrons below 2.5 GeV/c can be identified by the presence of a Čerenkov signal and K above 2.5 GeV/c by the absence of a Čerenkov pulse. The nitrogen data extended the electron identification to 5.6 GeV/c. This is summarized in Table 3.

Table 3

Data Summary		
Čerenkov Radiator	Isobutane	Nitrogen
$\int \mathcal{L}dt$ (pb^{-1})	94	22
Hadronic Events Detected	43 K	10 K
π Threshold (GeV/c)	2.6	5.6
K Threshold (GeV/c)	9.2	20
Average Number of Photoelectrons	26	5

4. Particle Fractions

10K hadronic events ($\int \mathcal{L}\,dt = 22$ pb^{-1}) with isobutane as the Čerenkov radiator have been analyzed to obtain the fraction of π, K and P.

Below 2 GeV/c, particles were identified using the TOF system. Even though the resolution is not sufficient to identify individual tracks, a statistical separation is possible. The measured mass-square (M^2) distribution of each momentum bin is fitted to the sum of three Gaussians to obtain the number of π, K and P. Such a fit is shown in Figure 5. These numbers are then corrected for decay, interaction and range-out, these corrections being done independently for $\pi^{\pm}$, $K^{\pm}$, P and $\overline{P}$. The corrected numbers are then normalized to get the particle fractions.

Above π threshold, the Čerenkov counter separates π from K and P; however, there is no separation between K and P.

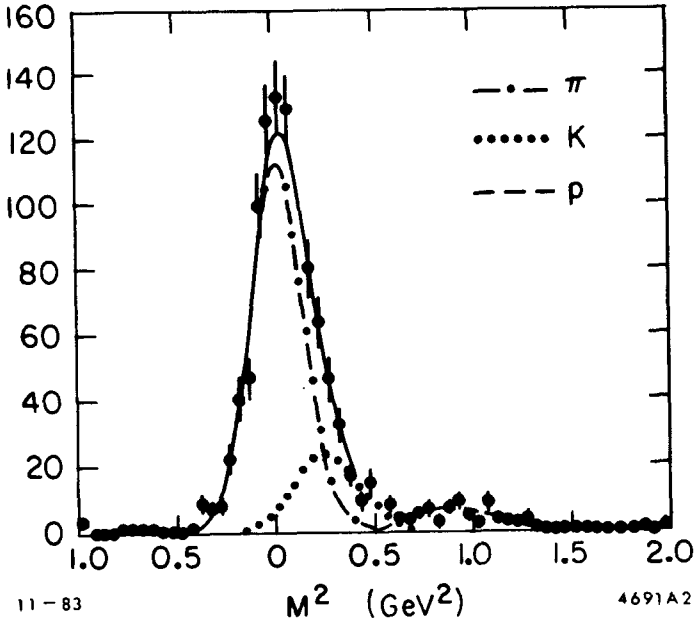

Figure 5 M^2 distribution for $0.3 < p < 0.4$ GeV/c. The solid line is the result of a fit to the sum of three Gaussians. The individual Gaussians are also shown.

The particle fractions in hadronic events are shown in Figure 6 as a function of momentum. Data from TASSO[1] at $\sqrt{s} = 34$ GeV are also shown for comparison.

3. Direct Electron

3.1 Introduction

We will use the term "direct electrons" to refer to those electrons which are the primary decay products of a heavy quark (c or b).

Direct electrons have a distinct signature. Their momentum (p) and transverse momentum (p_t) relative to the jet direction are characterized by the mass of the parent quark, while the electrons from γ-conversion, K-decay, et cetera, are usually much less energetic.

The branching ratio (BR) of a heavy quark to any individual hadronic decay mode is expected to be small because of the large number of available channels. However, the semileptonic BR is expected to be $\simeq$ 10%. Therefore, direct electrons are distinct and efficient tags of heavy quark flavors.

Previous measurements[2,3] of direct lepton production were generally restricted to $p > 1.5$ GeV/c (Figure 7); however, more than 1/2 of the electrons from c-quarks are expected to be below 2 GeV/c. DELCO's low-mass detector and Čerenkov counter extend this measurement to $p = 200$ MeV/c.

3.2 Electron Identification

Electrons are identified using Čerenkov and shower counters. Track curvature at low momenta leads to inefficiencies in the Čerenkov counter, while the upper momentum limit is determined by π threshold. Therefore electrons in the momentum range 200 (500) MeV/c to 2.5 (5.5) GeV/c can be identified when the radiator is isobutane (nitrogen). Electrons are required to have a minimum pulse height of 16 (1.8) photoelectrons. The signal is further required to be in-time within 1 nsec (1.5 nsec).

The shower counter response is required to be within two standard deviations of that expected from an electron. These two requirements were satisfied by 85 % of all electrons. The efficiency was determined using electrons from two-γ events.

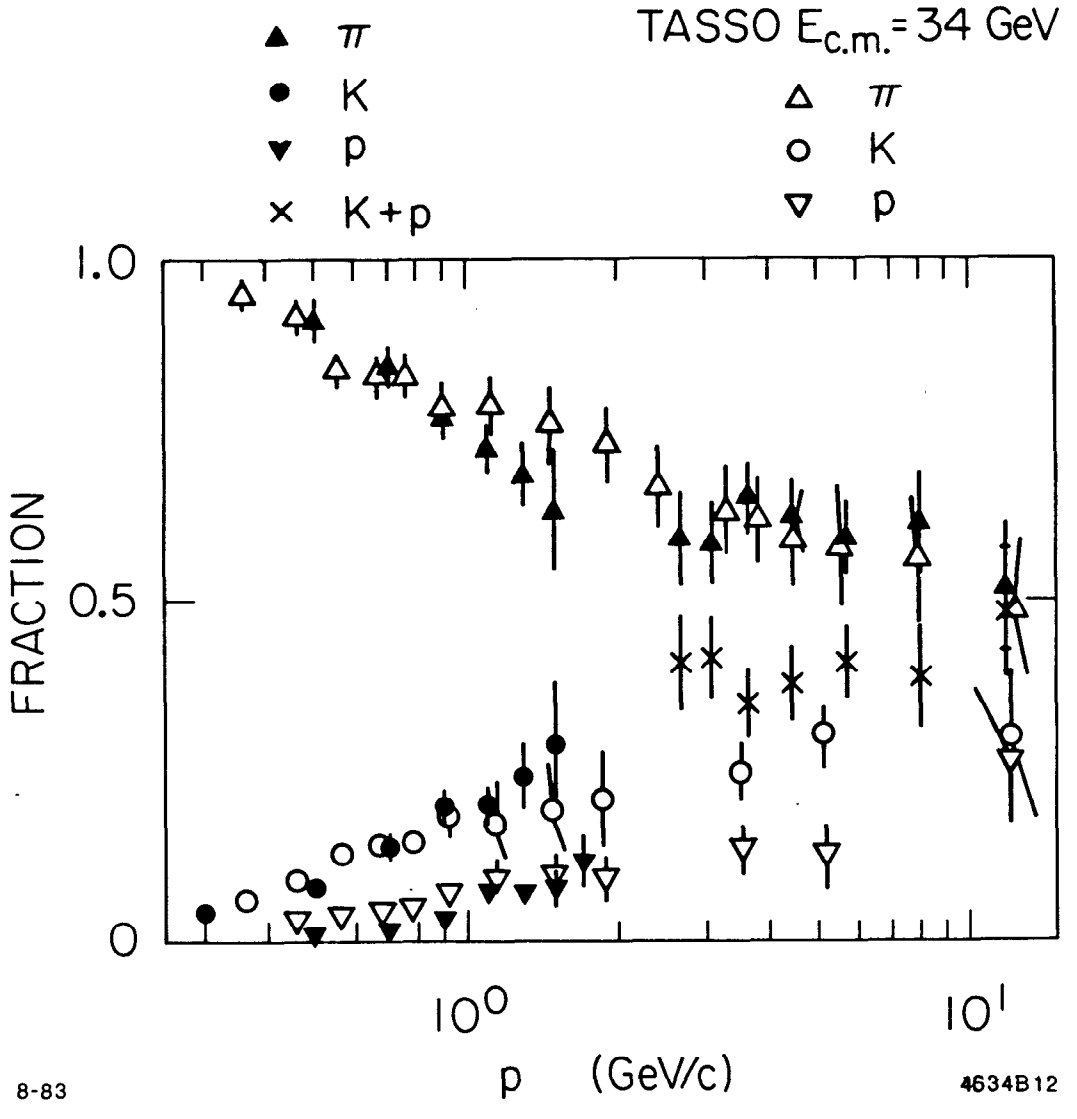

Figure 6 π, K and P fractions in hadronic events versus momentum. Data from TASSO at $\sqrt{s} = 34$ GeV are also shown.

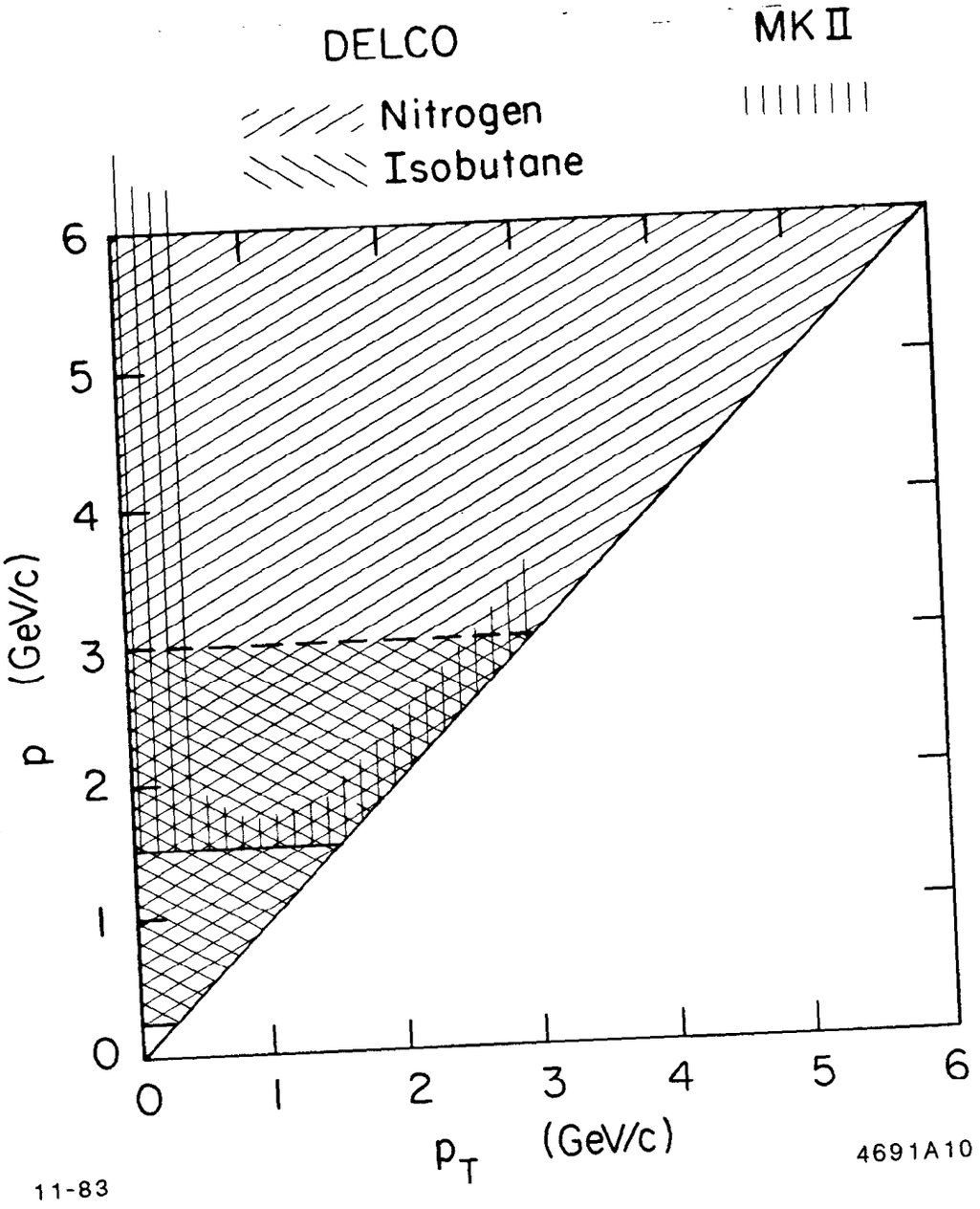

Figure 7 The momentum range covered in e^+e^- direct lepton production experiments. Other published results cover a range similar to MARK II.

3.3 Background Subtraction

There are two dominant backgrounds to the electron signal:

1. real electrons from γ–conversions and Dalitz decays, and
2. non-electron tracks whose counter response mimicked that of an electron, e.g., π traversing a Čerenkov cell which is fired by an undetected γ–conversion.

Much of the background is identified and removed event-by-event. The residual background is then subtracted statistically based on Monte Carlo predictions. This subtraction represents a 25% correction.

The number of γ–conversions is minimized by having little material (5 % X_0) before the Čerenkov counter. A γ–reconstruction program was used to identify and reject photons and Dalitz decays. The surviving events were hand-scanned for asymmetric conversions, where the momentum of one electron is too low to be reconstructed efficiently. The hand-scan is sensitive to tracks with momenta above 20 MeV/c. The residual γ background is subtracted statistically using the predictions of the Monte Carlo.

The non-electron background is primarily due to a hadron traversing a Čerenkov cell which was fired by a γ–conversion that occurred too late to be tracked in the inner drift chambers. However, uncorrelated track stubs in the outer drift chamber tag these late conversions. The residual background was calculated and subtracted. The Monte Carlo predictions were checked by "track-flipping". A track is reflected about the origin and the event re-analyzed to see if the new track would now be identified as an electron. Figure 8 compares the backgrounds calculated by these two methods for the same integrated luminosity.

There are other sources of background. Momentum mismeasurement of π above threshold, δ–ray and K–decay, were considered. They constitute a small background and have been subtracted.

3.4 Results

The differential cross-section $(d\sigma/dp)$for isobutane and nitrogen data are shown separately in Figure 9. Their agreement at low momenta (up to π threshold in isobutane) is good. The combined results are plotted in Figure 10, and compared with published results from MARK II.[2] There is an overall normalization uncertainty of 30 %.

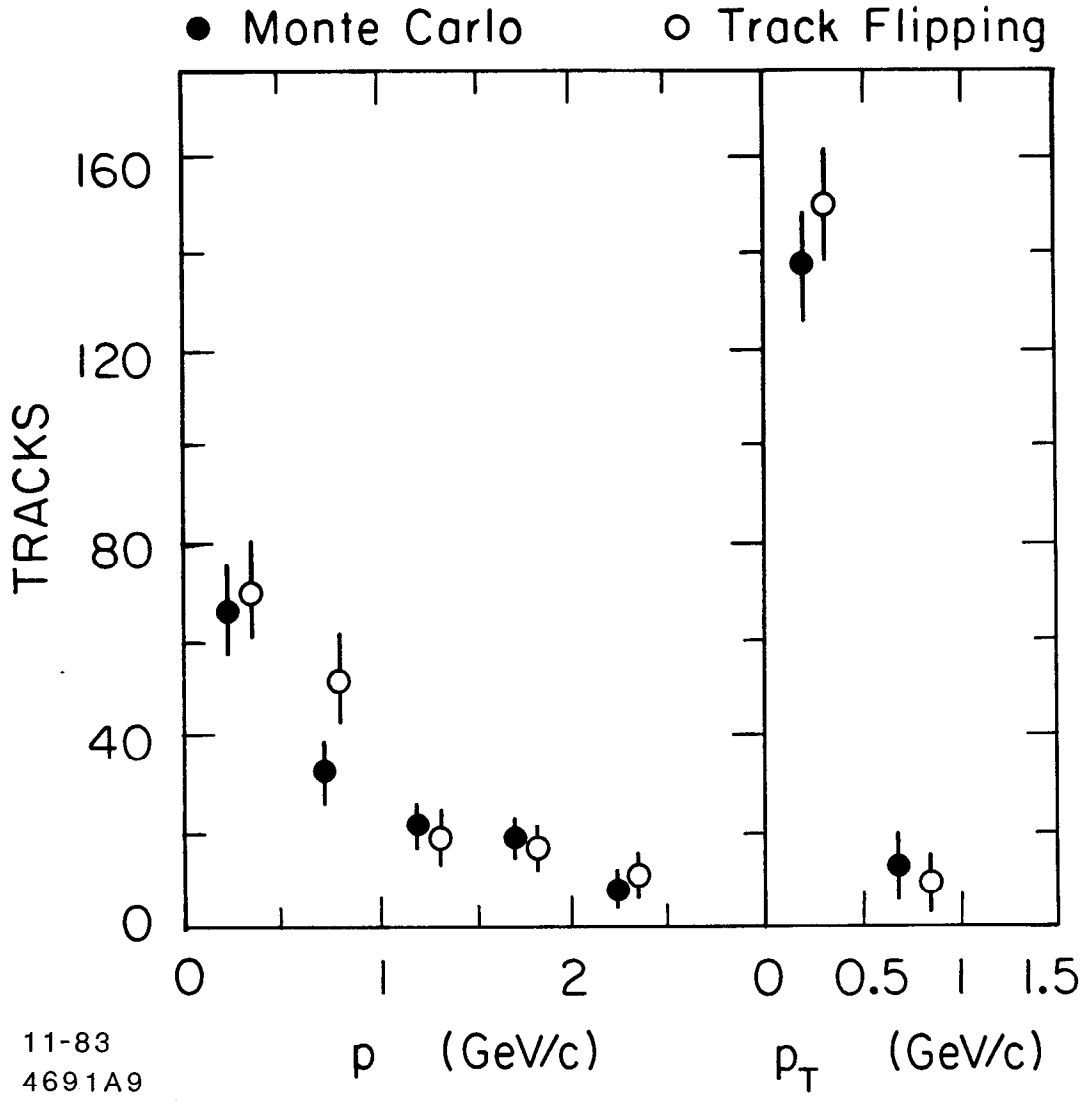

Figure 8 Comparison of background calculations from Monte Carlo and track-flipping techniques. The two calculations are for the same integrated luminosity.

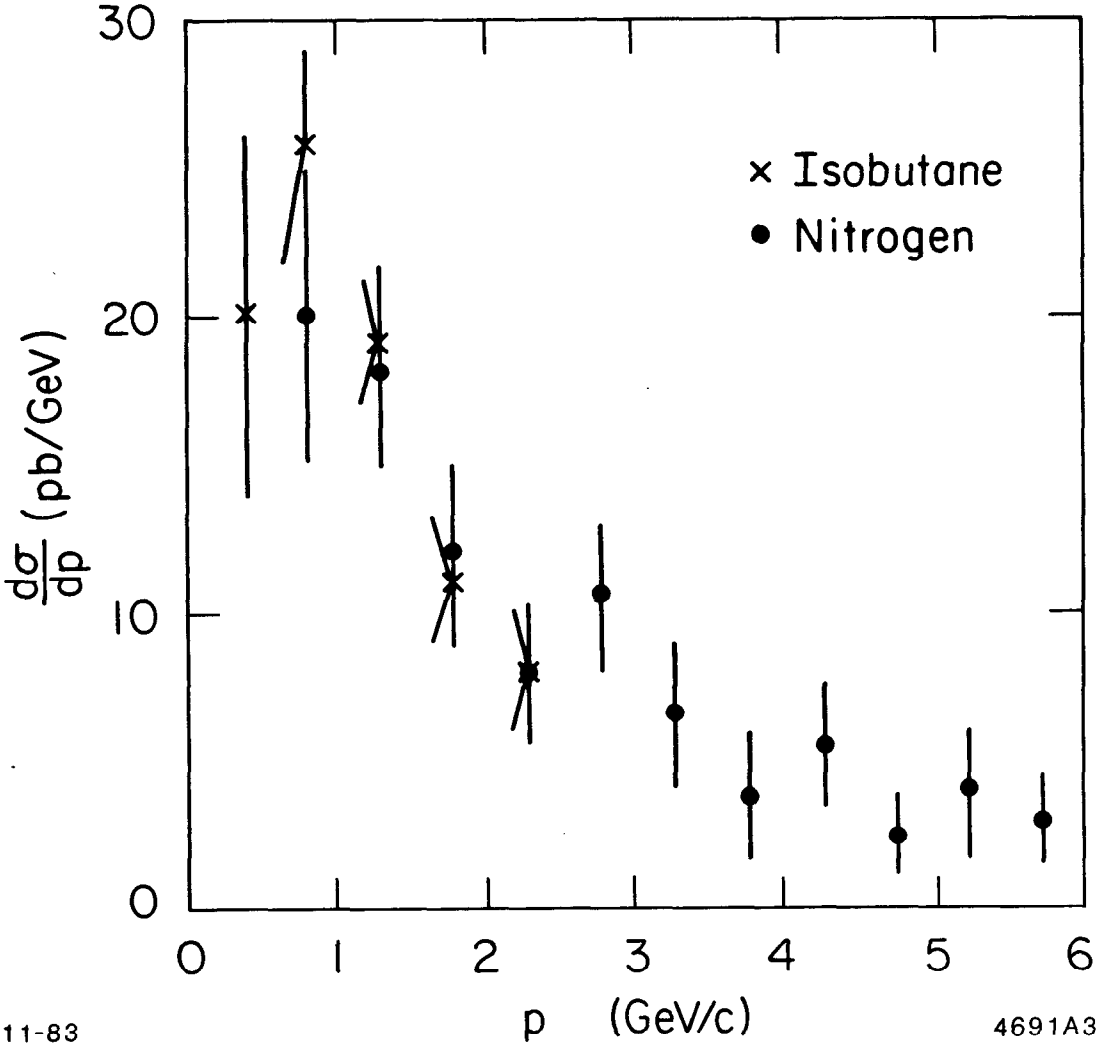

Figure 9 Differential cross-section of direct electrons. Isobutane and nitrogen data are shown separately.

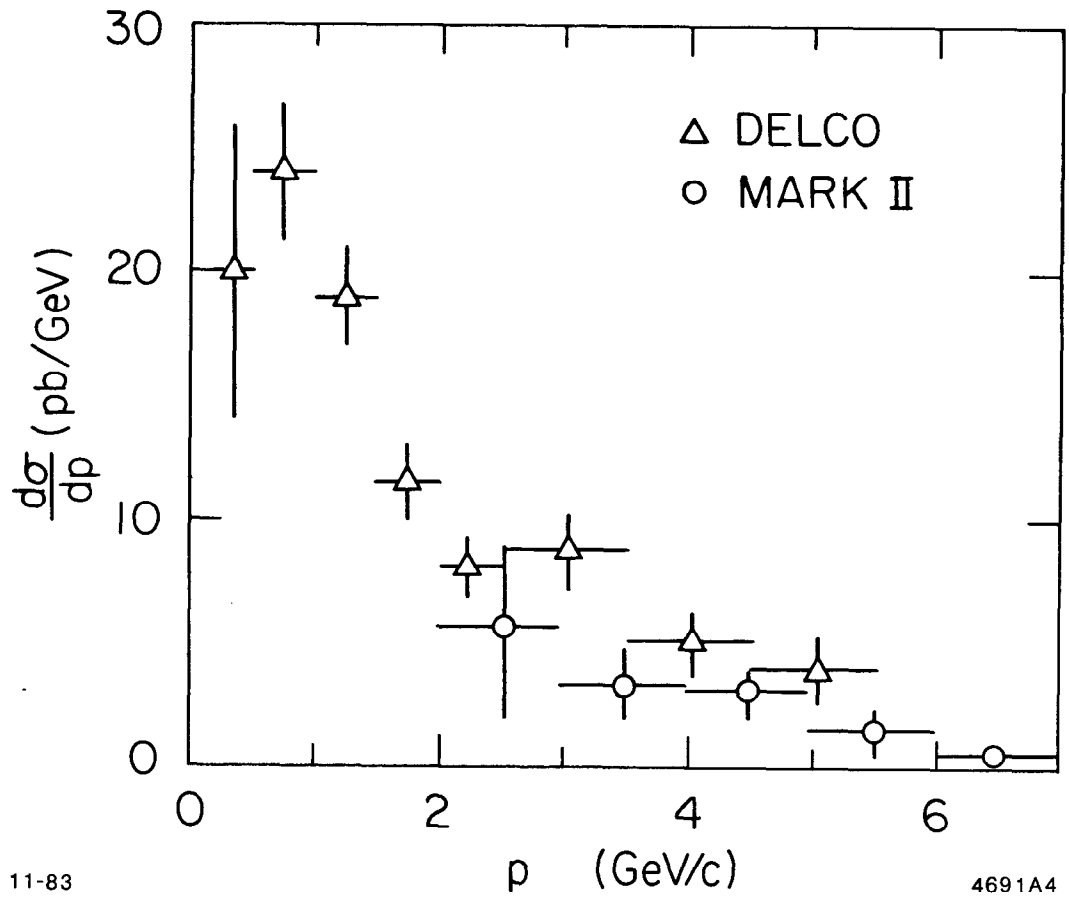

Figure 10 Comparison of $d\sigma/dp$ with MARK II results. There is an overall normalization uncertainty of 30% which is not included in the error bars.

Comparison with the prediction of the Lund Monte Carlo,[4] using the Peterson fragmentation function[5] for heavy quarks, is shown in Figure 11. However, the differential cross section is insensitive to the fragmentation function, and cannot be used to determine fragmentation parameters.

This distribution has been integrated to obtain the total cross-section, and the results are in Table 4. The cross section to produce a hadron with one or more direct electrons is σ_{1e}, and $R_{1e} = \sigma_{1e}/\sigma_{\mu\mu}$. The Lund Monte Carlo predicts $R_{1e} = 0.41$, integrated over all momenta.

Table 4

Total Cross Section to Produce Direct Electrons (The first uncertainty is statistical and the second is systematic.)		
Momentum Range	σ_{1e}	R_{1e}
$.2 < p < 2.5\,\mathrm{GeV/c}$	$36 \pm 2 \pm 10\,\mathrm{pb}$	$.35 \pm .0 \pm .07$
$.2 < p < 5.5\,\mathrm{GeV/c}$	$52 \pm 3 \pm 16\,\mathrm{pb}$	$.51 \pm .03 \pm .10$

3.3 Two-Electron Events

There are several conventional sources of two-electron events. They can be divided into four classes by their charge combinations and the jets that they belong to. Some conventionally expected sources are illustrated in Table 5.

Table 5

Some Conventional Sources of Two-Electron Events		
	Same Jet	Opposite Jet
Same Charge		$b \to c \to s\nu e^+$ $\bar{b} \to \bar{c}\,\nu e^+$
Opposite Charge	$b \to c\nu e^-$ $\hookrightarrow \quad s\nu e^+$	$c \to s\nu e^+$ $\bar{c} \to \bar{s}\,\nu e^-$

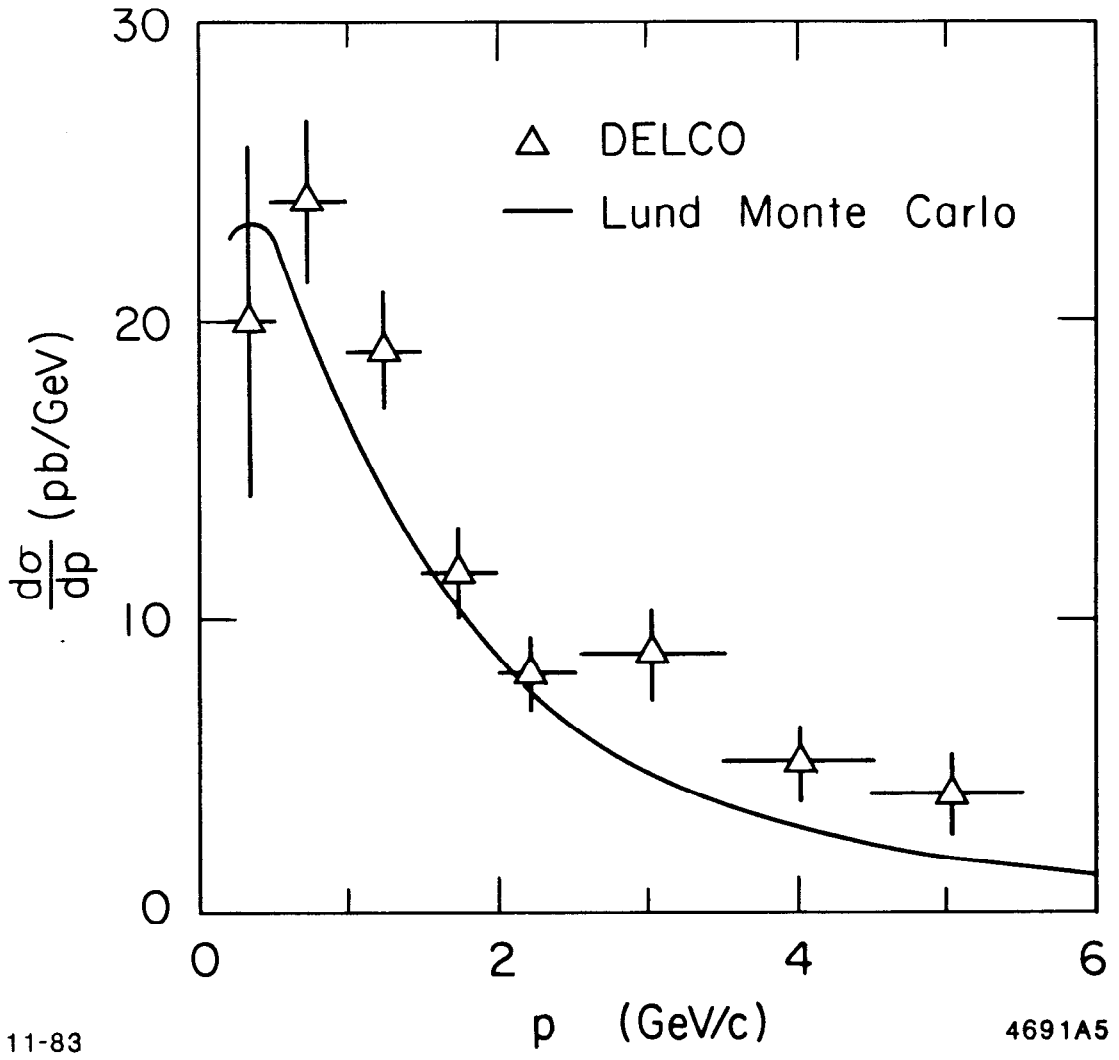

Figure 11 Comparison of $d\sigma/dp$ with predictions of the Lund Monte Carlo.

The background can be divided into two groups:

1. both electrons are background tracks;
2. one electron is a genuine direct electron, while the other track is background.

These background rates can be computed from the known genuine and background single electron rates obtained in the previous analysis. Ten background events are expected, and 26 events are found in 116 pb^{-1}.

This corresponds to a cross-section ratio $R_{2e} = (2.1 \pm .8 \pm 1.)\ 10^{-2}$, where the first uncertainty is statistical and the second one is systematic. In a model where $BR(b \to e) = 12\%$, $BR(c \to e) = 8\%$, $BR(b \to \tau \to e) = 1\%$, and neither B nor D mix, the cross-section ratio is predicted to be 3.8×10^{-2}.

The momentum distributions of the data and Monte Carlo are compared in Figure 12. The correlation matrix of the observed data is compared with the predicted signal plus background in Table 6. The comparisons show that the 'standard' model, as outlined above, is consistent with data. However, the preliminary nature of the data and its limited statistics preclude a detailed comparison.

Table 6

Comparison of Number of Two-Electron Events with Monte Carlo Predictions
(Background contributions are included in both sets of numbers.)

		Same Jet	Opposite Jet
Same Charge	(Data)	1	3
	(MC)	2	7
Opposite Charge	(Data)	9	12
	(MC)	4	13

4. D^* Production

4.1 INTRODUCTION

D^*'s have been detected[6,7] through the decay chain

$$D^{*+} \to D^0 + \pi^+$$
$$\hookrightarrow\ K^- + \pi^+ \quad .$$

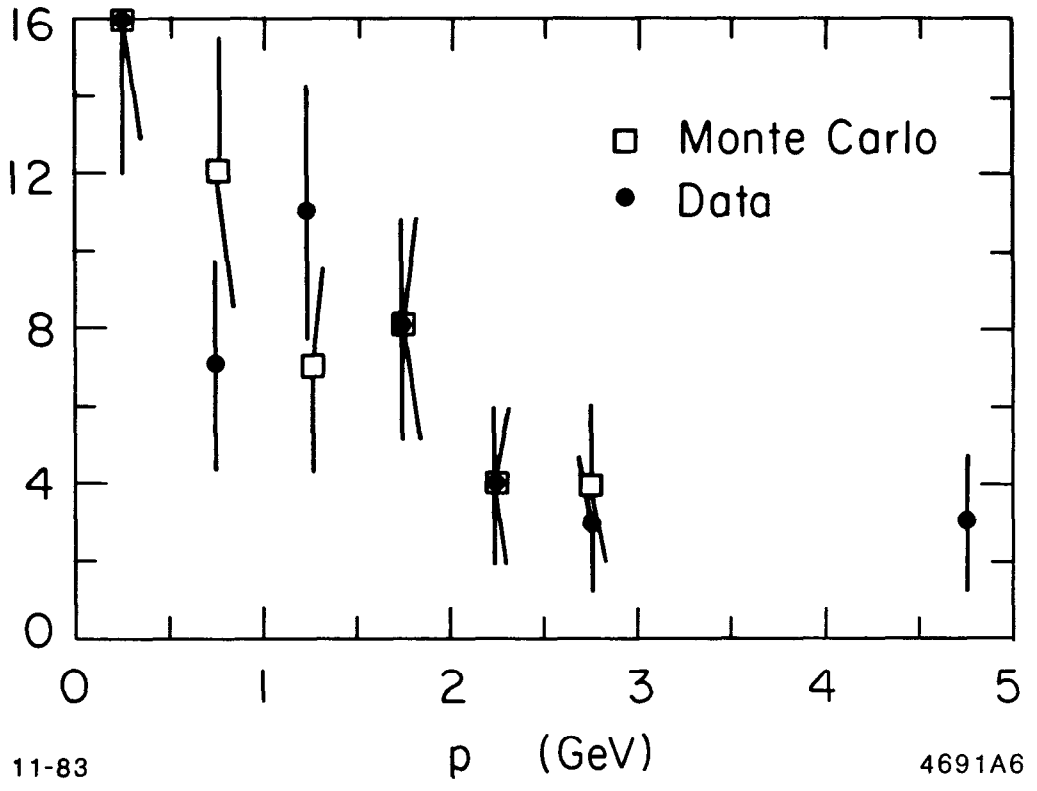

Figure 12 Comparison of Monte-Carlo and measured momentum distributions of two-electron events. Both distributions include background contributions.

The conjugate decay for D^{*-} is implied. The small Q value of the primary decay (6 MeV) leads to good resolution in the mass difference $\Delta M = M(D^*) - M(D^0)$. We have looked for D^*'s using several decays of the D^0, and will report on the total cross-section and fragmentation function.

4.2 ANALYSIS

A particle above π threshold is identified by the Čerenkov counter as a π or K by the presence or absence of a signal. It is then paired with all oppositely charged particles to make $(K^{\mp}\pi^{\pm})$ combinations. Those combinations with an invariant mass in the range 1.66 to 2.20 GeV are taken to be D^0 candidates. The energy of the D^0 is then calculated using the measured momenta and its known mass. The D^0 candidate is then paired with all appropriately charged π's, i.e., $(K^{\mp}\pi^{\pm})\pi^{\pm}$. The mass difference distribution (Figure 13) shows a distinct peak at the expected value.

The background due to random combinations is estimated using "wrong-sign" pions. Assuming no $D^0 - \overline{D^0}$ mixing, the pion from the initial D^* decay and the kaon should have opposite charge. D^0's were paired with wrong-sign pions and the resulting mass difference is also shown in Figure 13. This distribution shows no enhancement in the signal region, but is consistent with the right-sign data in the high mass region.

The background estimate was further checked by "track-flipping". The Čerenkov-identified track (K or π) is reflected about the origin, and the entire analysis repeated. Both the right-sign and wrong-sign pions should produce background events. There were 33 (28) events with the right (wrong) sign.

Several decay modes of the D^0 were examined:

1. $D^0 \rightarrow K^- + \pi^+$,
2. $D^0 \rightarrow K^- + \pi^+ + X$,
3. $D^0 \rightarrow K^- + \pi^+ + \pi^- + \pi^+$.

TOF identification of kaons was also used in the analysis of the first decay mode. Figure 14 is the mass difference distribution of TOF identified events.

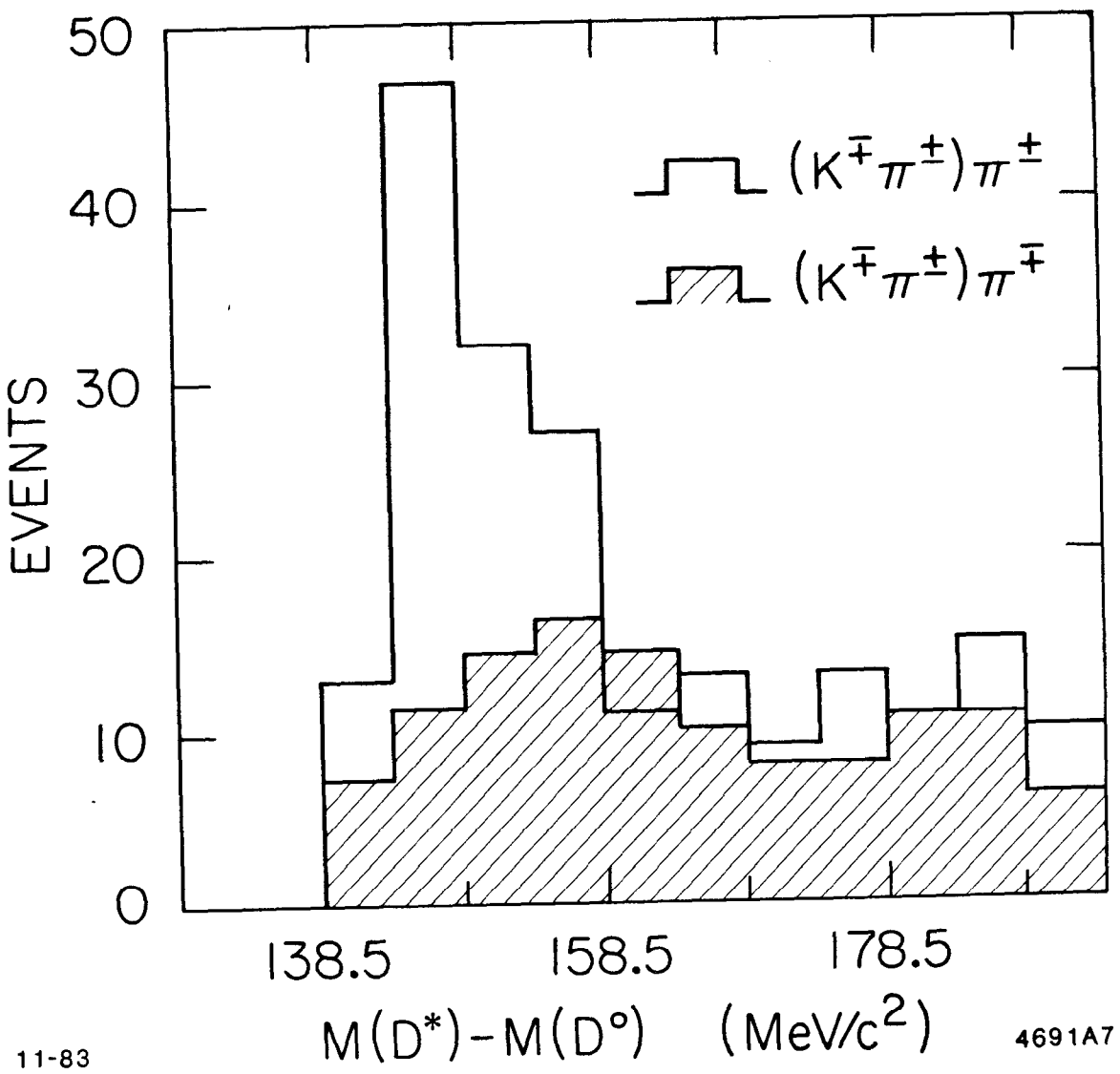

Figure 13 Mass difference $[M(D^*) - M(D^\circ)]$ distribution in $D^{*+} \to D^\circ\pi^+ \to K^-\pi^+\pi^+$ where the K is Čerenkov-identified. The background, as measured by wrong-sign π, is indicated in the shaded region.

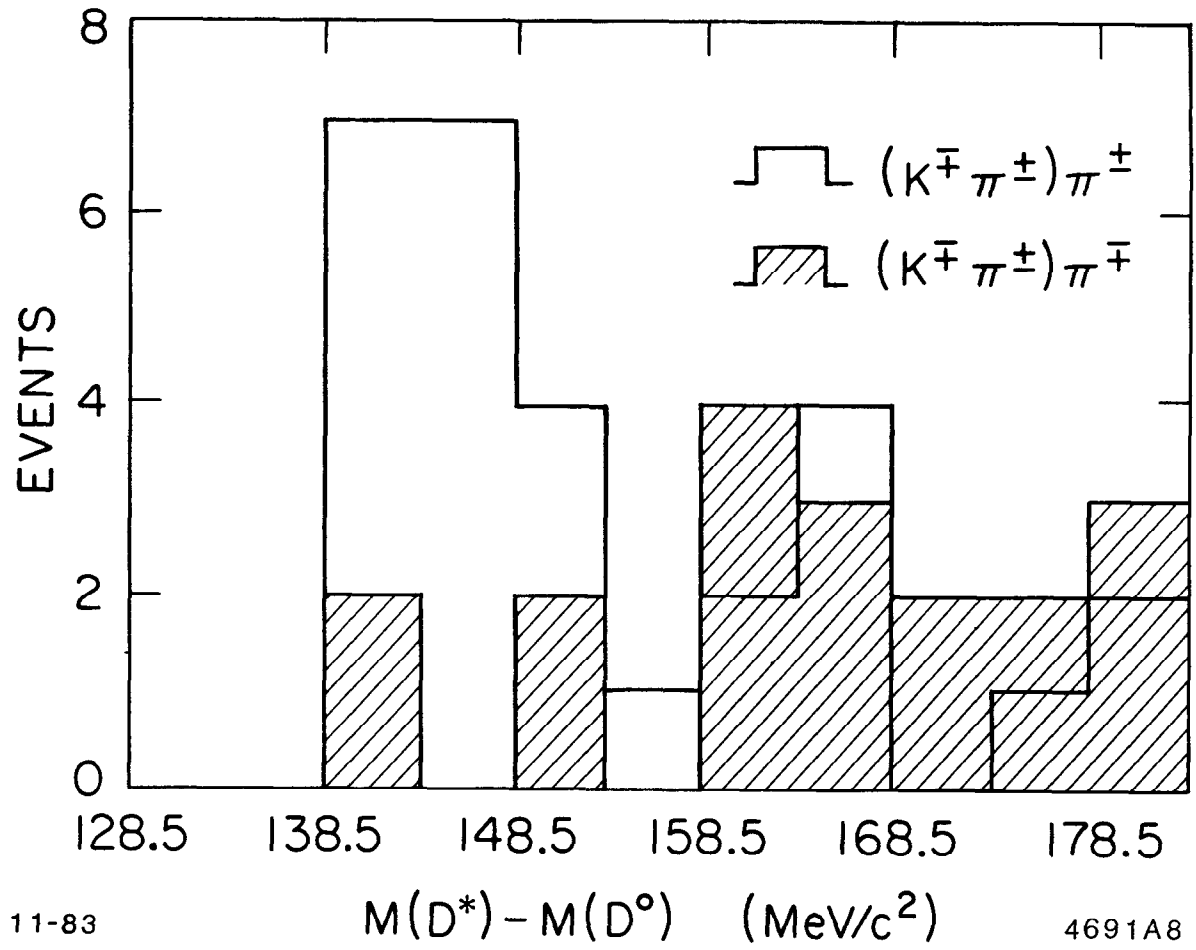

Figure 14 Mass difference $[M(D^*) - M(D^\circ)]$ distribution in $D^{*+} \rightarrow D^\circ\pi^+ \rightarrow K^-\pi^+\pi^+$ where the K is TOF-identified. The background, as measured by wrong-sign π, is indicated in the shaded region.

4.3 RESULTS

After correcting for detection efficiencies (Figure 15) and branching ratios[8] (Table 7), the total cross-section is obtained for each of the 3 decay modes used. The results are summarized in Table 8. The data span the entire kinematically allowed momentum range, and a measurement of the total cross-section is possible without an extrapolation.

Table 7

Branching Ratios Used in Calculating Total Cross Sections	
Decay Mode	BR
$D^{*+} \to D^{\circ} + \pi^{+}$	0.44
$D^{\circ} \to K^{-}\pi^{+}$	0.03
$D^{\circ} \to K^{-}\pi^{+}X$	0.072
$D^{\circ} \to K^{-}(3\pi)^{+}$	0.085

Table 8

Total Cross Section to Produce $D^{*\pm}$ at $\sqrt{s} = 29$ GeV (The first uncertainty is statistical and the second is systematic.)	
D° Decay Mode	$\sigma(D^{*\pm})$ (nb)
$K\pi$	$.152 \pm .026$
$K\pi X$	$.151 \pm .029$
$K3\pi$	$.151 \pm .025$
Average	$.151 \pm .020 \pm .040$

The average value of $0.151 \pm .020 \pm .040$ nb is compared with published results in Table 9.

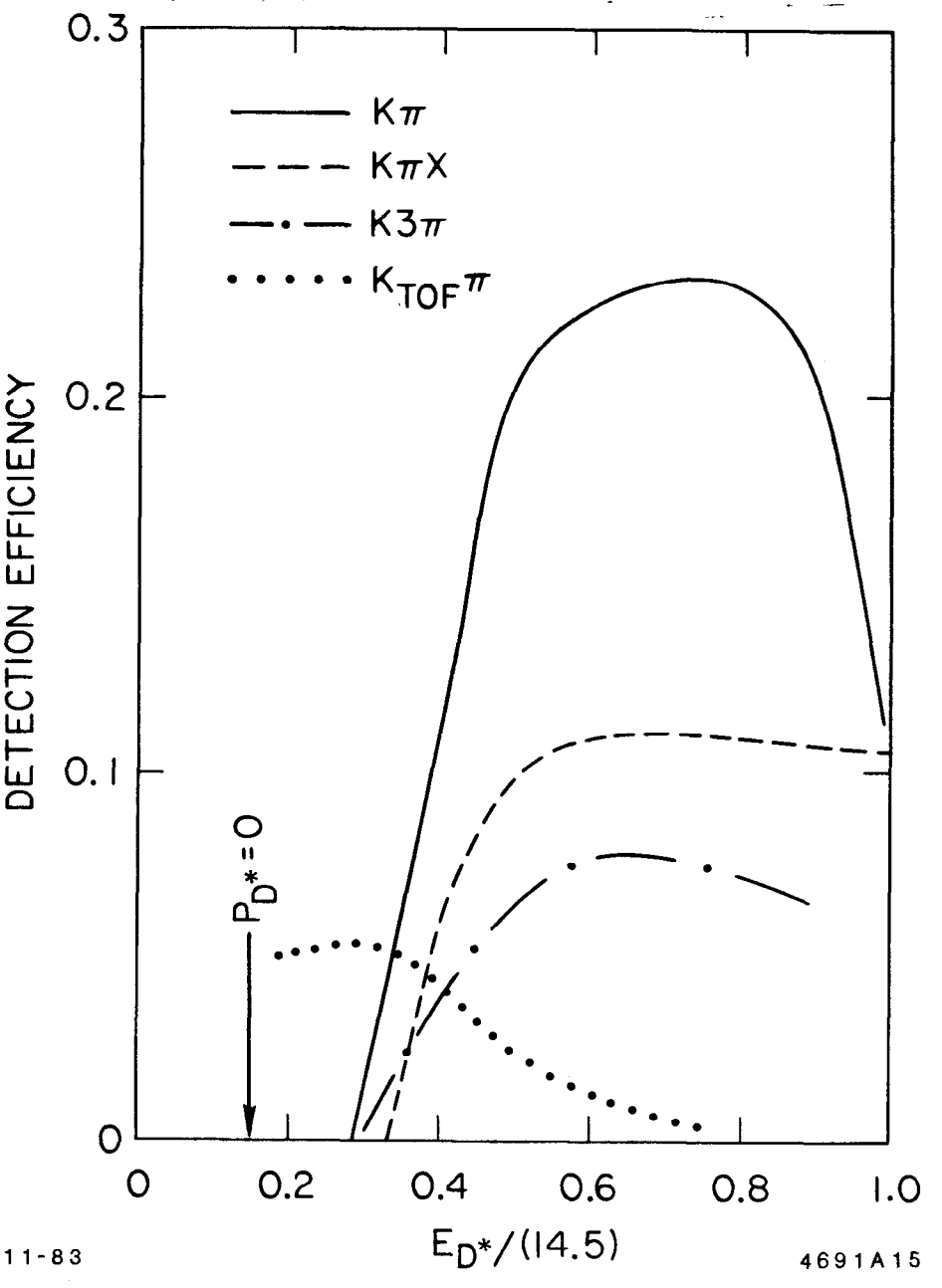

Figure 15 D^* detection efficiency as a function of E_{D^*}/E_{beam} for three D° decay modes.

Table 9

Comparison of D^* Total Cross Section with MARK II and TASSO Measurements	
Experiment	$\sigma(D^{*\pm})$ (nb)
This Experiment	$0.151 \pm .020 \pm .040$
MARK II[6]	0.25 ± 0.13
TASSO[7]	$0.20 \pm 0.05 \pm 0.07$

The differential cross-section, $d\sigma/dx$ where $x = E_{D^*}/E_{beam}$, is compared with MARK II and TASSO data in Figure 16. The lowest x point uses TOF-identified K's, and has a normalization uncertainty of 30% relative to the other data points. When this distribution is fitted to the function[5]

$$f(x) = 1/x(1 - 1/x - \epsilon/(1-x))^{-2}$$

one obtains $\epsilon = 0.79$. See Figure 17.

It should be emphasized that the quark fragmentation function is a function of $z = E_{D^*}/E_{quark}$ and not x. The effects of initial state photon radiation and gluon bremsstrahlung are to soften the observed momentum distribution. These effects were simulated and the contribution of b quarks was taken into account by assuming $\epsilon_q \alpha\, 1/M_q$. The predictions for three different values of ϵ are shown in Figure 18. The data do not show a strong preference for a particular value of ϵ.

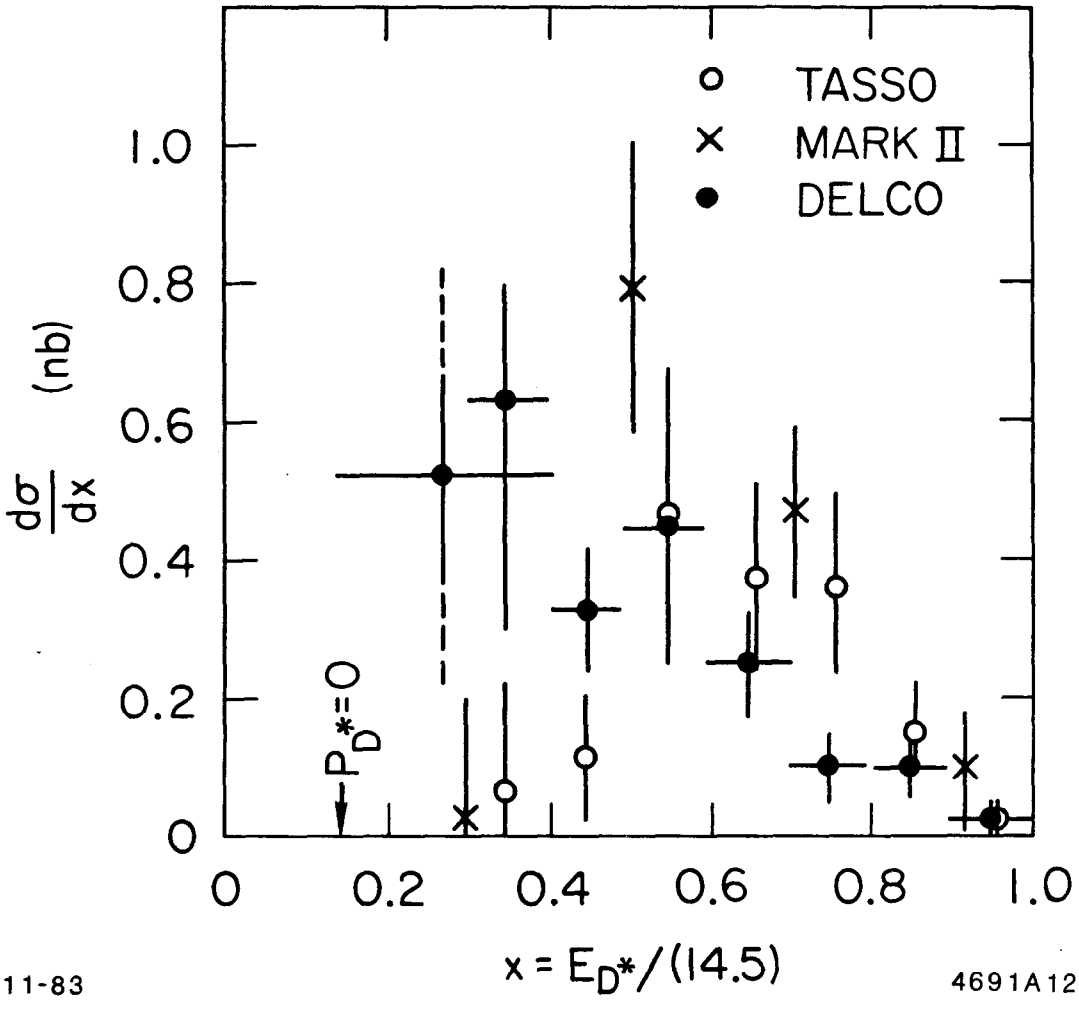

Figure 16 Comparison of $d\sigma/dx$, where $x = E_{D^*}/E_{beam}$, with MARK II and TASSO results. Except for the data at $x = 0.25$, the errors do not include relative normalization uncertainties. The DELCO data at $x = 0.25$ use TOF-identified K's and have a normalization uncertainty of 30% relative to the other DELCO data points. This is shown by the dashed lines.

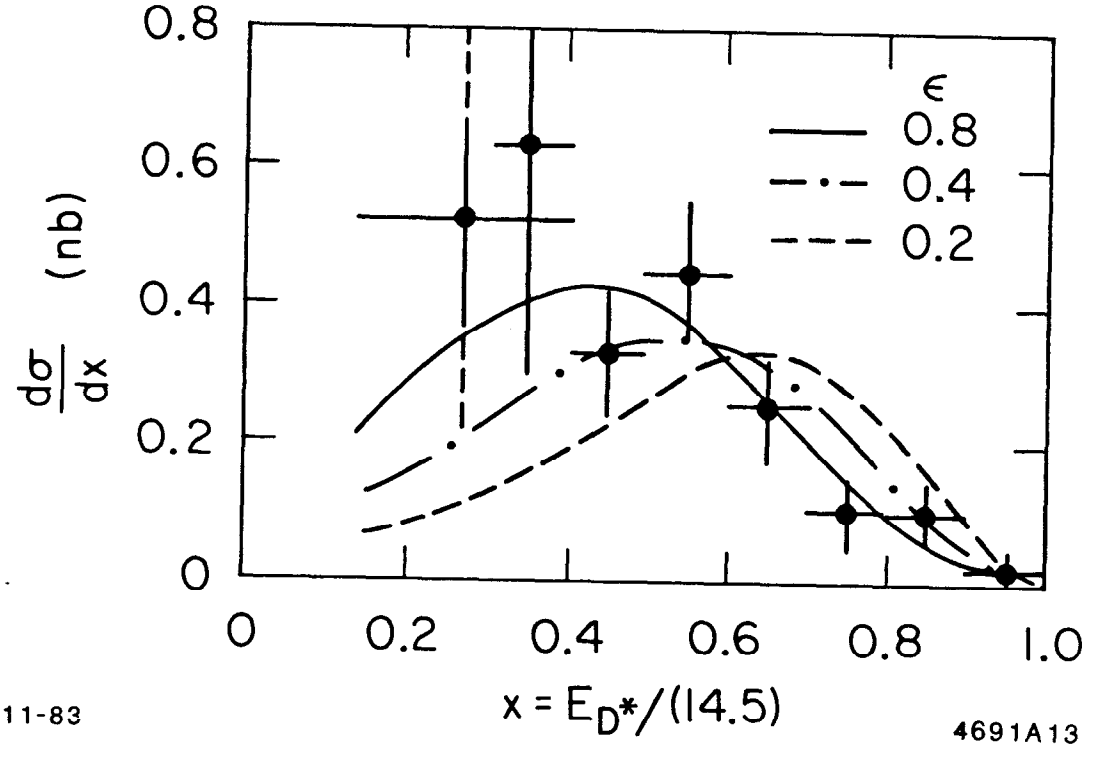

Figure 17 Comparison of $d\sigma/dx$ with the function $f(x) = 1/x[1 - 1/x - \epsilon/(1-x)]^{-2}$ for three values of ϵ. The best fit is obtained with $\epsilon = 0.79$.

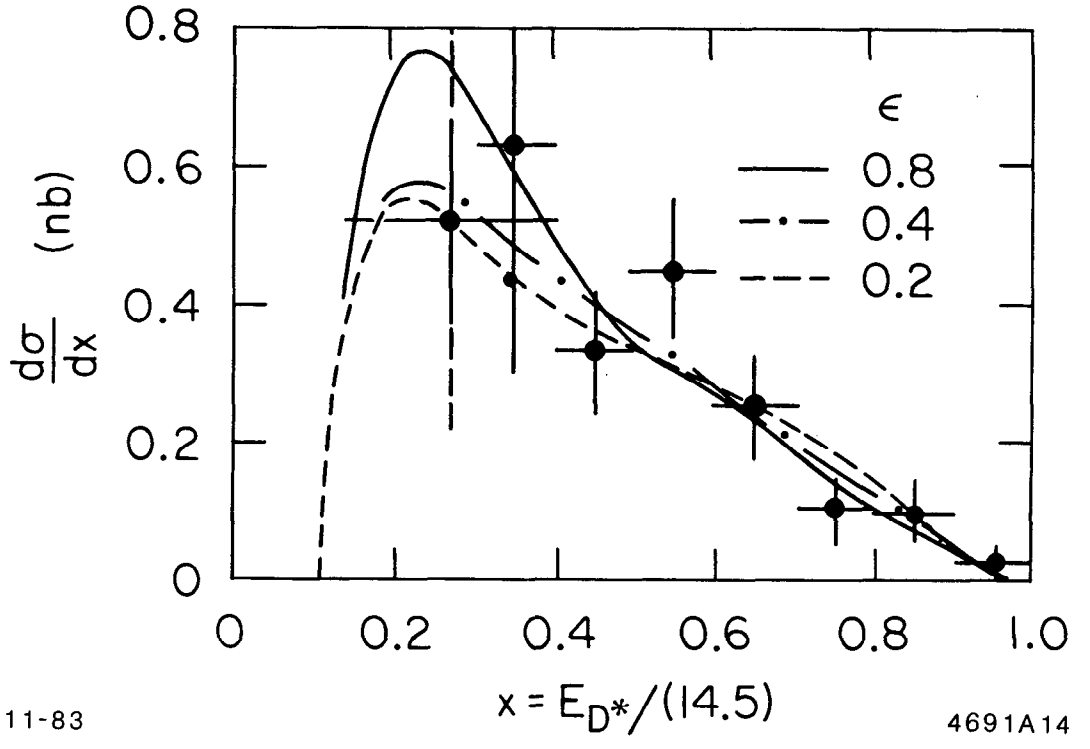

Figure 18 Comparison of $d\sigma/dx$ with predictions using a fragmentation function of the form

$$f(z) = 1/z[1 - 1/z - \epsilon/(1-z)]^{-2} \quad .$$

The effects of initial state radiation and gluon Bremsstrahlung, as well as the contributions of b-quark are included. Three values of ϵ for the c-quark are shown.

References

1. M. Althoff *et al.*, Z. Phys. C17, 5 (1983).
2. Previous measurements of direct electron production in e^+e^- collisions: M. E. Nelson *et al.*, Phys. Rev. Lett. 50, 1542 (1983); H. J. Behrends *et al.*, Z. Phys. C19, 291 (1983).
3. Previous measurements of direct muon production in e^+e^- collisions: E. Fernandez *et al.*, Phys. Rev. Lett. 50, 2054 (1983); W. Bartel *et al.*, Phys. Lett. 99B, 277 (1981); B. Adeva *et al.*, Phys. Rev. Lett. 51, 443 (1983).
4. T. Sjostrand, Comput. Phys. Commun. 28, 229 (1983).
5. C. Peterson *et al.*, Phys. Rev. D27, 105 (1983).
6. J. M. Yelton *et al.*, Phys. Rev. Lett. 49, 430 (1983).
7. M. Althoff *et al.*, Phys. Lett. 126B, 493 (1983).
8. Particle Data Group, LBL-91 (1983). Note that some analyses have assumed $BR(D^{*+} \to D^0 + \pi^+) = 0.66$ instead of 0.44.